

Confinement Induced Alteration in Interfacial Energy

Nitish Singh^{1,#}, Arka Roy^{1,#} and Animangsu Ghatak^{1,2,*}

[1] Department of Chemical Engineering, Indian Institute of Technology Kanpur, 208016

[2] Center for Environmental Science and Engineering, Indian Institute of Technology Kanpur, 208016 (India)

[*] Prof. A. Ghatak, Corresponding-Author, Author-Three, E-mail: aghatak@iitk.ac.in

[#] Both authors contributed equally

Hypothesis: When a liquid is confined between two parallel plates, the pressure field at its bulk alters, because of the concave meniscus at the air-water interface. For an aqueous surfactant solution in contact with an oil, like an oil-in-water emulsion, this effect can alter the surfactant concentration at the interface of the two phases thereby changing the interfacial energy. Alteration of interfacial energy is expected to affect morphology of a complex system consisting of three immiscible phases.

Experiments: A drop of crosslinkable silicone liquid was placed on a glass slide and was immobilized by partial crosslinking. An aqueous solution of surfactant, with SiO₂ microspheres dispersed in it, was dispensed on this drop to create a liquid pool. It was then confined between two parallel plates to create a meniscus.

Finding: Consequently, the particles got embedded at the oil-water interface to different extent, depending on the degree of confinement. Force balance along tangents to different interfaces showed that the interfacial energy of silicone-water (aqCTAB 0.3 mM) interface increases from $33.3 \pm 0.5 \text{ mJ/m}^2$ for an unconfined system to $45.4 \pm 2.2 \text{ mJ/m}^2$ for the confined one. This effect then elucidates how confinement alters complex emulsion morphologies in multiphase systems.

Key words: interfacial energy, dispersed particles, complex emulsion, confinement

Introduction:

When a liquid layer is confined between two parallel plates with wettable surface, a concave meniscus appears at the liquid-air interface [1]. Across this meniscus, there occurs a pressure difference, associated with the surface tension of the liquid, known as the Laplace pressure. Because of this effect, the pressure at the liquid side of the meniscus decreases below the atmospheric pressure thereby altering the pressure field within the liquid [1]. Question arises how such alteration in pressure in the bulk liquid would affect the energetics of an interface submerged within it, for example the liquid-liquid interface of an emulsion or a solid-liquid interface of dispersion of particles. This question is important for large number of practical applications, e.g. efficiency of particle separation in a froth floatation cell [2], complex emulsions in pharmaceutical, food and beverage and wellness-product industry [3, 4, 5], alteration in morphology of complex emulsion, e.g. core-shell to Janus [1, 6] morphology of droplets of dispersed phase within the a continuous liquid, generation of pickering emulsion [7, 8], generation of complex adhesives embedded with viscoelastic domains [9], generation of adaptable optical lenses via emulsion route [10] and so on. While in most these examples, behavior of the bulk liquid under the influence of various internal and external factors like temperature [16], light [17], pH [18] has been studied in detail, how exactly confinement of the bulk liquid would affect the dynamics of a phenomena, or the equilibrium morphology of a buried interface has not been examined in any detail.

It is to address this question that we have presented here an experiment in which migration of colloidal particles, dispersed within a liquid, to the interface with another liquid, has been examined under varying degree of confinement. In essence, here we have a partially crosslinked drop of silicone submerged within a pool of aqueous solution of a surfactant, thereby mimicking an oil in water emulsion. The aqueous phase contains also suspended colloidal silica (SiO_2) microspheres. We show that when we confine this liquid dispersion between two parallel plates, the colloidal particles migrate to the oil-water interface and get

adsorbed within it forming a contact angle which is different from that for an unconfined system. In fact, this effect varies systematically with the degree of confinement thereby signaling a change in the energy of an interface buried within. Manifestation of this phenomenon was visible also in a complex emulsion consisting of three immiscible phases, in which alteration in its confinement triggered change in morphology of the emulsion drops. Our controlled experiments, performed in absence of surfactant molecules in the bulk liquid, didn't show the above effects. These results confirmed that confinement induced alteration in pressure field results in desorption of surfactant molecules from the oil-water interface which increases the interfacial energy and triggers consequent migration of particles to the interface.

Materials and Methods:

Materials:

SiO₂ microparticles (diameter: 9-13 μm) and Trichloro(1H,1H,2H,2H-perfluorooctyl) silane (FC) were procured from Sigma Aldrich. Paraffin Oil (0.830 – 0.880 gm/ml at 20°C), Silicone Oil (330-370 cSt) and N-Cetyl-N,N,N Trimethyl Ammonium Bromide 99% (CTAB) and Agarose were procured from Loba Chemie Private Limited, and sodium lauryl sulphate (SDS) was bought from Fisher Scientific. Liquid silicone rubber (LSR) was used as the oil phase and was purchased from Momentive. Single cavity-glass slides were bought from AIM Scientific. The chemicals were used as received without purification. In all experiments, degasified DI water was used for preparing samples.

Method:

Preparation of degasified water: Preparation of degasified water: Method of preparation of degassed water has been described in reference [11]. Briefly, deionized water was first, purged with Nitrogen gas (N₂) for 30 min, following which, water was refrigerated for 24 hours. The ice was then thawed and brought to room temperature; it was further heated to 45°C and subsequently cooled to room temperature. It was purged again with N₂ for another 30 mins.

Finally, this water was degassed at ~ 10 milli bar vacuum pressure for 1-2 minutes before preparing any sample.

Preparation of Glass slides: The single cavity-glass slide was cleaned thoroughly using ethanol-water after being treated in Piranha solution (70%v/v H₂SO₄ + 30%v/v H₂O₂) for 5-6 hours. This plate was coated with a self-assembled monolayer (SAM) of FC molecules by the conventional dip coating method. In brief, the glass plate was first plasma-oxidized (4 minutes of plasma and 1 minute of oxygen) at 1-2 milli bar vacuum pressure inside a Harrick Plasma cleaner. Then this plate was submerged inside a pool of Toluene consisting of FC molecules at 1:1000 v/v ratio for 4-5 hours, during which the FC molecules chemisorbed on the glass surface. After removing them from the solution, they were cleaned thoroughly with ethanol-water. This oleophobic glass slide ensured that the silicone drop forms a finite contact angle on it and after curing, the crosslinked lens detaches easily from the slide.

Preparation of silicone drop: LSR was mixed with curing agent (10% w/w), degasified in a vacuum chamber at ~ 1-2 milli bar pressure for 3 to 4 minutes; 0.3 to 0.5 ml of this liquid was dispensed as a sessile drop on the cavity of the FC functionalized glass slide using a micropipette tip (figure 1a,b). Due to the oleophobic effect of the FC surface, the droplet formed a spherical lens (of diameter 0.7 to 1.2 mm), with advancing contact angle of ~60°, as shown in figure 1(c). The maximum height of drops was 0.2 - 0.3 mm so that they were small enough to get accommodated within the cavity of height 0.35 - 0.4 mm. Yet, the drop was much larger in size than that of the SiO₂ microspheres which implied that the particles essentially interacted with a flat silicone surface and didn't feel the effect of its curvature.

Preparation of aqueous dispersion of SiO₂ microspheres: Aqueous solutions of 1 mM SDS (aqSDS) and 0.3 mM CTAB (aqCTAB) solutions were prepared by mixing required amount of the respective surfactant in DI water. Magnetic stirring was used for mixing CTAB and SDS in water, whereas Agarose powder was dissolved in water at elevated temperature inside a

microwave oven. SiO₂ particles were dispersed in the surfactant solution at concentration of 0.5 mg/ml (figure 1b); to make a uniform dispersion, the liquid was subjected to sonication for 10 to 15 minutes. It was then immediately used for further experiments.

Preparation of complex emulsion: The process of making complex emulsion has been described in detail in reference [1]. In brief three immiscible liquids: paraffin oil, silicone oil (330-370 cst) and aqueous surfactant solution were taken at 1:2:10 v/v ratio. First the paraffin oil was dispersed in the surfactant solution by stirring it at 10000 rpm for 1 min to form a simple emulsion. Then the silicone oil was added to it while stirring the liquid at 10,000 to 12,000 rpm for ~10 min. This process resulted in a complex emulsion with core-shell droplets dispersed in the aqueous phase: paraffin oil at the core and silicone oil at the shell. The core-shell morphology altered to Janus morphology when a small quantity of the emulsion was confined between two parallel plates with sufficiently small gap in-between.

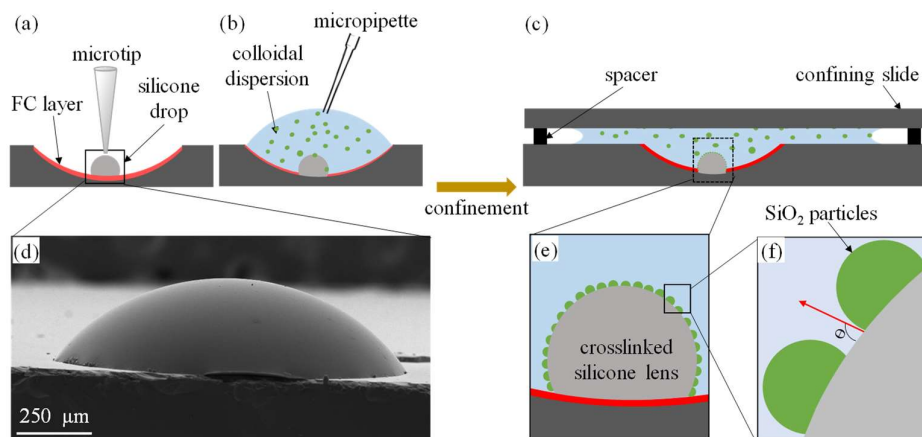


Figure 1: (a-c) The schematic depicts the sequence of steps in the experiment in which a drop of silicone (mixed with the curing agent) was first dispensed on an FC-coated single cavity glass slide. Followed by it, the silicone drop was immobilized by crosslinking to a limited extent and then a small quantity of aqueous dispersion of SiO₂ microspheres was released into the cavity using a micropipette. The liquid pool was confined by placing another glass slide on top of it; the slides at the top and bottom were kept uniformly separated by placing two spacers of equal thickness between them. (d) The scanning

electron microscopy image represents a typical crosslinked silicone lens on the glass slide with cavity. (e, f) Schematic of SiO₂ particles embedded on the silicone surface and its magnified view.

Method of carrying out the particle-probe experiment: The silicone liquid drop was allowed to crosslink partially for 35 - 45 minutes at 25° C temperature, which rendered it immobile on the glass surface. The glass plate with the silicone lens on it, was then flooded with the aqueous surfactant solution dispersed with the SiO₂ particles and the liquid pool thus formed, was sandwiched by placing another glass slide from top (Figure 1c); two spacers of identical thickness were placed between the slides, at their two ends, to create a uniform gap between the slides (figure 2a-d). Preliminary experiments showed that a drop of uncrosslinked silicone tends to get displaced while confining the liquid pool. On the other hand, if the silicone gets completely crosslinked, the interfacial effect that we wish to probe, can't kick in. Therefore, the silicone drop was crosslinked only sufficiently that it remained liquid like, yet didn't flow out during the course of the experiment (figure 1d). The extent of confinement was varied by using spacers of thickness varied from $h = 5$ mm to 50 μ m between the two glass slides. The gap between the plates could not be reduced further as it was difficult to form a meniscus without flooding also the spacers. Care was taken also that the top slide does not contact the silicone drop immobilized on the bottom slide. The whole set-up was kept inside a chamber with controlled humidity to prevent any evaporation of water from the sandwiched layer. After 2 hours, during which the silicone crosslinked completely, the top glass slide was removed, the slide with the crosslinked silicone lens attached to it was washed off the aqueous phase. In a second set of experiments, the pool of liquid containing the particles was left unconfined. In both these experiments, the SiO₂ microspheres were expected to migrate to the interface with the silicone and get embedded into it but to different extent depending on the degree of confinement (figure 1e,f). It is known that interfacial energy of silicone alters with change in environment because of switching of its molecular configuration [19]. Therefore, to ensure that

such alteration in interfacial energy doesn't lead to release of the adsorbed SiO₂ microspheres, the silicone lens along with the glass slide was stored inside the aqueous solution of the same surfactant in which it was first crosslinked; this liquid was devoid of any SiO₂ microspheres in it.

Preparation of samples for SEM imaging: Before carrying out SEM of the silicone lenses, the glass slide, with the silicone lens adhered to it, was first withdrawn from the liquid pool in which it was stored, was rinsed thoroughly with DI water and was blow dried with Nitrogen gas. The lens was then transferred to a second piece of glass slide (0.5 cm X 1cm) with the help of a sharp surgical blade which was placed vertically and was then coated with gold using sputter coater to attain a thickness of ~5 nm. The side view of this lenses were captured using ZEISS EVO 18 SEM.

Results and discussion:

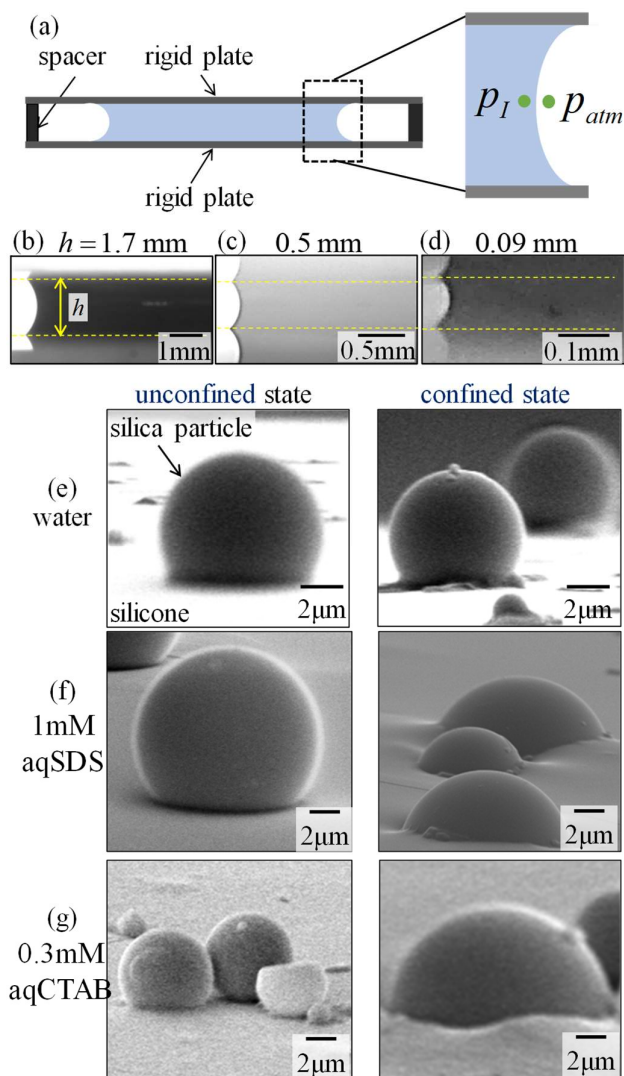


Figure 2: (a) Schematic shows the formation of a meniscus at air-liquid interface when a puddle of liquid is confined with two glass slides separated by spacers of desired thickness. The Laplace pressure across the concave meniscus creates pressure field in the liquid below atmospheric. (b-d) The optical images show the menisci for confinement heights 1.7 mm, 0.5 mm and 0.09 mm respectively. (e-g) Scanning electron micrographs (SEM) show SiO₂ particles embedded on silicone elastomer lens for three different aqueous medium: water, 1mM aqSDS and 0.3 mM aqCTAB solutions. In each case, images at left

and right panels represent respectively the unconfined ($h_{unconfined} = 5\text{ mm}$) and confined state ($h_{confined} = 50\text{ }\mu\text{m}$).

Effect of confinement on particle migration to the silicone-aqueous (SA) interface: Figure 2e-g summarise the results which show that SiO₂ microspheres get adsorbed on the silicone-water interface to different extent depending on the extent of confinement of the liquid pool. Three different aqueous media were used for forming the liquid pool and in each case, the SEM images of the particles showed the effect of confinement. The sequence of images (e-g) represents the SEM of silicone lenses with particles embedded in it. For the image of figure 2(e), the aqueous dispersion of SiO₂ particles was devoid of any surfactant. When this liquid was used to form the pool on the silicone drop, the particles were found to get embedded into the silicone to the identical extent for the both confined and unconfined liquid pool. In other word, confinement driven alteration of pressure field within the liquid pool didn't alter the interfacial energy of the silicone-water interface in absence of surfactant in the aqueous phase. On the other hand, when an aqueous solution of a surfactant, e.g. 1 mM aqSDS was used as the liquid pool, the particles were found to get embedded to different extents for the confined and unconfined states (Figure 2f). In the confined state, the particles got embedded into the silicone to a larger extent than when the liquid pool was unconfined. Similar was the observation for 0.3mM aqCTAB solution (figure 2g), thereby emphasizing the point that this phenomenon occurred irrespective of the type of surfactant used, provided that the liquid pool was sufficiently confined. Furthermore, this phenomenon was observed irrespective also of size of particles. The SEM images in figure S3 show that for a 0.3mM aqCTAB solution, SiO₂ particles of wide-ranging sizes: $\sim 5 - 15\text{ }\mu\text{m}$ got embedded to identical extent to the silicone lens in the confined and unconfined state respectively. To examine further, if the trapping of the SiO₂ particles was driven by gravity induced settling, the arrangement as in figure 1(c) was flipped upside down, so that the cavity slide with the pendant drop of silicone now remained on top

(figure 3a); 1 mM aqSDS with SiO₂ particles dispersed in it, was used as the liquid pool as before. The experiment was done in both unconfined and confined states and here too the SiO₂ particles got embedded into the silicone in the same way as before. The SEM images in figure 3(b,c) show that at the unconfined state, the particles were hardly trapped; whereas, in the confined state, the extent to which the particles got embedded into silicone, was similar to that in the figure 2(f). These observations buttressed the point that it was the confinement of the liquid pool that determined the extent of entrapment for the particles within the silicone layer: with increase in confinement of the liquid pool, the wettability of the particles increased.

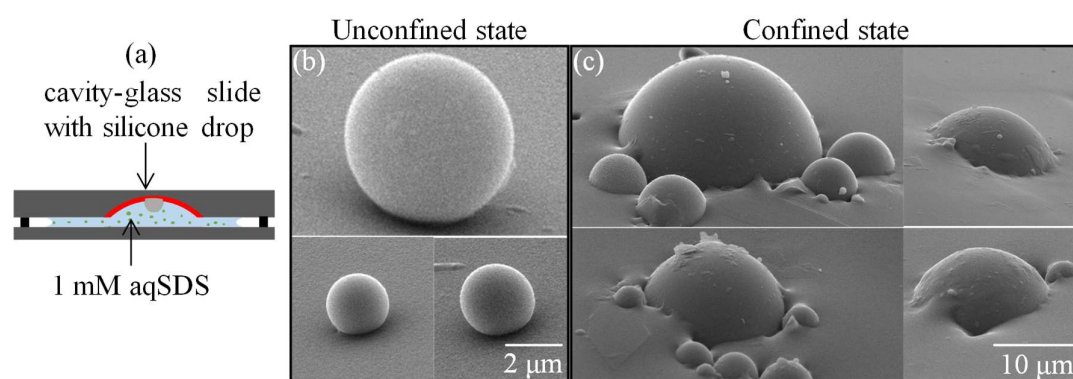


Figure 3. (a) Schematic of experiment in which the silicone drop was placed upside down by flipping the arrangement of figure 1(c). 1mM aqSDS was used as the liquid pool, in which the silicone drop was kept immersed. SiO₂ particles were dispersed in the liquid pool. (b, c) The images, representing SEM micrographs of SiO₂ particles bonded to the silicone lens correspond respectively to the unconfined and confined states of the liquid pool.

To quantify these observations, angle between tangents drawn at different interfaces were measured. It was noted that for the unconfined state, the silicone surface was almost flat and undeformed as shown in the schematic of figure 4(a). In contrast, for the confined state, the silicone surface appeared undeformed away from the particle, but was deformed at the vicinity of it (figure 4b). The tangents were drawn accordingly, with γ_{12} representing interfacial tension

between silicone and aqueous medium and γ_{p1} and γ_{p2} representing those at the particle-silicone and particle-aqueous medium interface respectively. It is worth noting here that tangents γ_{p1} and γ_{p2} appear co-linear because of the spherical shape of the particle.

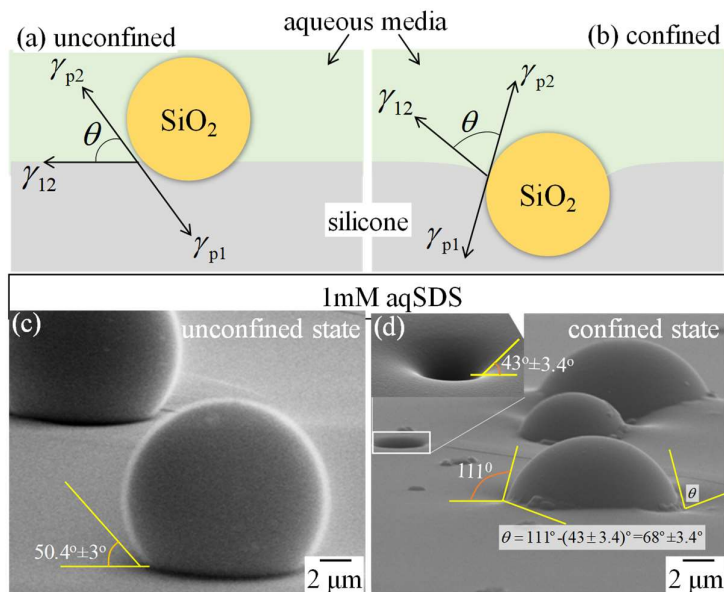


Figure 4. (a, b) The figures show schematic representation of SiO₂ microspheres embedded inside the silicone surface for the unconfined and confined case respectively. Tangents drawn along different interfaces depict the balance of interfacial forces. (c, d) Images depict angle between tangents drawn along different interfaces. Set of images correspond to 1mM aqSDS solution. The images show also the angle between tangents drawn along the silicone-aqueous medium and particle-aqueous medium interface. For any given system, this angle was found nearly identical for different particles. For the unconfined state, angle θ between the SiO₂ micro-sphere and the silicone surface is found to be $50.4^{\circ} \pm 3^{\circ}$ and that for the confined state is found to be $68^{\circ} \pm 3.4^{\circ}$.

Figure 4(c, d) show the tangents drawn at different interfaces and angle θ shows that between tangents corresponding to γ_{12} and γ_{p2} . For the aqueous medium without any surfactant, θ was found to be $66^{\circ} \pm 2^{\circ}$ irrespective of the confinement of the liquid pool. On the other hand, for

aqueous solution of surfactant, θ was remarkably different for the confined and unconfined state. For example, in the case of aqSDS it increased from $52^\circ \pm 4^\circ$ at unconfined state to $114^\circ \pm 4^\circ$ when the liquid pool was confined.

aqueous phase	$\gamma_{\text{SiO}_2\text{-Sil}}$ (mJ/m ²)	$\gamma_{\text{SiO}_2\text{-aq}}$ (mJ/m ²)	Unconfined State		Confined State	
			θ (deg)	$\gamma_{\text{Sil-aq}} _{\text{unconfined}}$ (mJ/m ²)	θ (deg)	$\gamma_{\text{Sil-aq}} _{\text{confined}}$ (mJ/m ²)
Water	19.3	3.6	66.8 ± 2.3	40.2 ± 4.0	65.5 ± 1.3	38.1 ± 1.9
1mM SDS		1.7	51.7 ± 3.5	28.6 ± 2.2	113.7 ± 3.8	49.6 ± 9.3
0.3mM CTAB		1.4	57.3 ± 0.6	33.3 ± 0.5	111.7 ± 1.2	45.4 ± 2.2

Table 1: SEM images as in figure 4 are used to estimate the interfacial energy of SiO₂-aq and SiO₂-Sil interface at the unconfined and confined state respectively.

Estimation of interfacial energy

The interfacial energy, $\gamma_{\text{Sil-aq}}$ of the silicone-aqueous (SA) interface can be obtained by balancing forces [13] represented by tangents drawn along different interfaces as shown in figure 4(c, d). For example, from the known values of interfacial energy of particle-aqueous solution, $\gamma_{\text{SiO}_2\text{-aq}}$ and particle-silicone $\gamma_{\text{SiO}_2\text{-Sil}}$ interfaces and the measured value of angle θ , the angle between tangents drawn at particle-medium 1 and particle-medium 2 interfaces, $\gamma_{\text{Sil-aq}}$

can be written as $\gamma_{\text{Sil-aq}} = \frac{\gamma_{\text{SiO}_2\text{-Sil}} - \gamma_{\text{SiO}_2\text{-aq}}}{\cos \theta}$, which essentially is the Young's equation [12].

Surface energy components of SiO₂ particles, aqueous media and silicone material have been listed in Table S1. From these values, $\gamma_{\text{SiO}_2\text{-aq}}$ and $\gamma_{\text{SiO}_2\text{-Sil}}$ are estimated using Owens and Wendt equation [20] as detailed in Table S2. Using these values of $\gamma_{\text{SiO}_2\text{-aq}}$ and $\gamma_{\text{SiO}_2\text{-Sil}}$, and the angle between tangents drawn at particle aqueous medium interface and silicone-aqueous medium

interface as in figure 4, $\gamma_{\text{Sil-aq}}$ was estimated. Table 1 summarizes these results for experiments carried out at confined and unconfined state respectively. For water, without any surfactant in it, the interfacial energy, $\gamma_{\text{Sil-aq}}$ does not differ from confined to unconfined state of the experiment. However, $\gamma_{\text{Sil-aq}}$ becomes significantly different for the confined and unconfined states (Table 1). For example, for 1mM aqSDS solution, it increases from $28.6 \pm 2.2 \text{ mJ/m}^2$ at unconfined state to $49.6 \pm 9.3 \text{ mJ/m}^2$ for the confined case. Similarly for 0.3mM aqCTAB solution, it increases from $33.3 \pm 0.5 \text{ mJ/m}^2$ to $45.4 \pm 2.2 \text{ mJ/m}^2$ for unconfined to confined state of the experiment. Detailed calculations of interfacial energies are presented in Table S3.

Possible mechanism of alteration in interfacial energy:

Alteration in interfacial energy of silicone-aqueous (SA) interface in presence of surfactant molecules suggest that this phenomenon is essentially mediated by adsorption / desorption of the surfactant molecules at the interface. In fact, the surfactant concentration at the SA interface is expected to remain at equilibrium with the pressure field in the bulk liquid. When the pressure in the liquid pool increases, more surfactant molecules is expected to get adsorbed at the interface; desorption is expected when the pressure gets diminished because of the concave meniscus at the air-water interface in confined state. The schematic in Figure 5(a-d) presents a qualitative picture of this phenomenon. Here, decrease in concentration of surfactant at the SA interface, increases its interfacial energy and therefore, its ability to wet the colloidal SiO₂ microspheres. As a result, the particles now get embedded into the silicone phase to a larger extent. This equilibrium between interfacial concentration of surfactant at the interface and the bulk however alters, when the surfactant concentration at the bulk aqueous phase exceeds the critical micelle concentration (CMC). In fact, CMC presents a limit on the range of surfactant concentration in the aqueous phase, within which the above effect is expected to be observed. Noting that the CMC of aqSDS and aqCTAB are $\sim 8.25 \text{ mM}$ [23] and 1 mM [24] respectively, experiments were carried at surfactant concentration above these values. For example, for 10

mM aqSDS, γ_{aqSDS} was measured to be 35 mJ/m², for which, the interfacial energy of silicone elastomer and the surfactant solution was found to diminish to ~ 7 mJ/m² (Supporting information, Figure S2). Similarly, for 3mM aqCTAB, the interfacial energy of SA interface was estimated to be ~ 4 mJ/m². Such small value suggests that the interface was already at a state of low energy, at which its ability to wet the SiO₂ microspheres diminished significantly. SEM images in Figure 5(e-i), for experiments carried out at unconfined state, show that as the surfactant concentration increases in the aqueous media, the extent of deposition of SiO₂ microspheres on silicone surface decreases. Almost no particle gets adsorbed for surfactant concentration exceeding CMC (figure 5g,i). Confinement of this liquid pool doesn't alter this state, as now, a new equilibrium gets established between the SA interface, the bulk aqueous phase and the micelle phase. Micelles act as the reservoir of surfactant molecules and their effect dominates over the pressure field within the bulk liquid. In other word, increase in confinement diminishes the pressure in the aqueous medium, but the equilibrium between micelles and the bulk liquid ensures that no net desorption of surfactant molecules from the SA interface occurs and the interfacial energy of SA interface, and consequently its ability to wet the SiO₂ microspheres, does not increase.

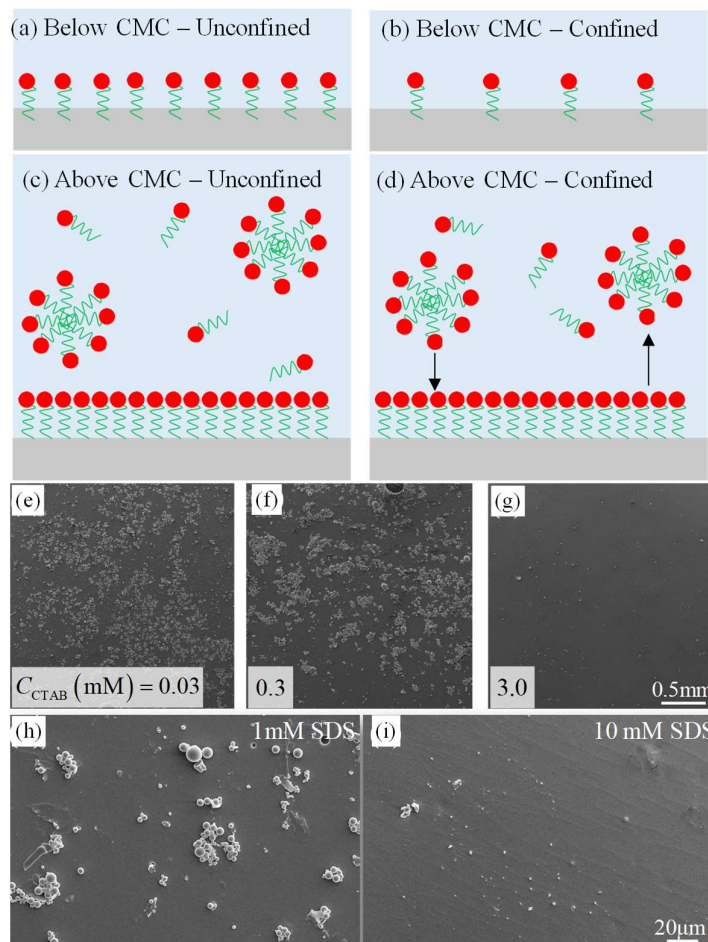


Figure 5: The schematic diagrams (a and c) show the arrangement of surfactant molecules at the silicone/aqueous media interface without confinement, while (b and d) show the arrangement with confinement, both above and below the critical micelle concentration (CMC). (e-i) SEM micrographs show the particles adsorbed on Silicone elastomer at the unconfined state of the experiment depicted in figure 1. Here, surfactant solutions of increasing concentration were used. Images e-g represent respectively 0.03 mM, 0.3 mM and 3 mM aqCTAB and h-i represent respectively 1 mM and 10 mM aqSDS.

Effect of confinement on interfacial energy at a liquid-liquid interface:

So far, we focussed on alteration in interfacial energy of a crosslinked solid and a liquid (aqueous surfactant solution) driven by effect of confinement. We will now show that similar effect can be observed also at a liquid-liquid interface, particularly in the context of complex

emulsion. Experiments [1] show that when an emulsion consisting of three immiscible liquids, e.g. paraffin, silicone as dispersed phases and aqueous solution of a surfactant (used as emulsion stabilizer) as the continuous phase, is confined between two parallel plates as in figure 2(c), the core-shell morphology of the emulsion droplets, with paraffin as core and silicone as the shell, change to the Janus morphology. Figure S4 shows that in the absence of a surfactant, the emulsion destabilizes leading to phase separation. Figure 6 illustrates such morphological transitions in presence of a surfactant in the aqueous medium: 1mM SDS (figure 6a,b), 0.3mM CTAB (figure 6c,d), and 0.1% Agarose (figure 6e). In all these cases core-shell morphology with paraffin and the core and silicone at shell is the energetically favourable one at the unconfined state. For example, for the 1mM aqSDS-paraffin oil-silicone oil system, the interfacial tension of various interfaces are, $\gamma_{\text{Par-aq}} = 41.44$ mN/m, $\gamma_{\text{Sil-aq}} = 31$ mN/m and $\gamma_{\text{Par-Sil}} = 0.78$ mN/m (Table 2) which results in the spreading coefficient, $S = \gamma_{\text{Par-aq}} - \gamma_{\text{Sil-aq}} - \gamma_{\text{Par-Sil}} > 0$. Positive S leads to formation of core-shell morphology with paraffin oil at the core and silicone oil at the shell. Furthermore, appearance of this morphology remains independent of the relative quantity of the two liquids as expected. When this emulsion is sufficiently confined as in figure 6(a,c), core-shell alters to Janus morphology (figure 6b,d) signifying that at this state, this morphology was the energetically favoured one, i.e. spreading coefficient, $S < 0$. To examine if it is indeed so, an estimate of $\gamma_{\text{Sil-aq}}$ and $\gamma_{\text{Par-aq}}$ were obtained by measuring the angles between tangents representing different interfacial tensions and by balancing the horizontal and vertical component of forces as in figure 6e. These angles (Table 2) can be related to interfacial tension values [15] by the following equation:

$$\cos \theta_A = \frac{\gamma_{BI}^2 - \gamma_{AI}^2 - \gamma_{AB}^2}{2\gamma_{BI}\gamma_{AB}} \text{ and } \cos \theta_B = \frac{\gamma_{AI}^2 - \gamma_{BI}^2 - \gamma_{AB}^2}{2\gamma_{AI}\gamma_{AB}}$$

Here I, A and B represent respectively the aqueous medium, paraffin oil and silicone oil. The $\gamma_{\text{Sil-aq}}$ values estimated from these relations (Table 2), were used to obtain S , which show that S was indeed negative for this Janus

morphology. S turned negative for other surfactants as well at the confined state. It is worth noting that $\gamma_{\text{Sil-aq}}$ increased significantly at the confined state; for 1mM SDS solution, it increased from 31 mN/m at the unconfined to 40.9 mN/m (Table 2) at the confined state. Such alteration in the interfacial tension values couldn't have occurred without desorption of the surfactant molecules from the silicone-aqueous media interface.

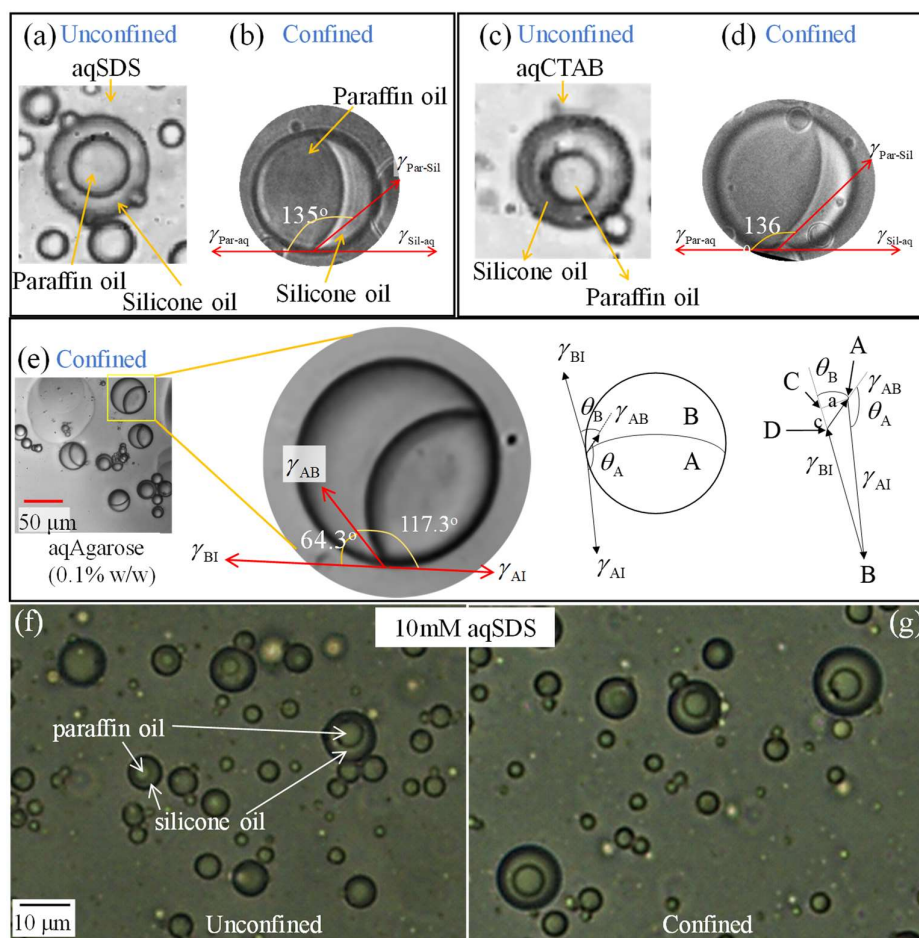


Figure 6: Images (a) and (c) shows the optical micrograph of core-shell droplet of a complex emulsion in aqSDS and aqCTAB respectively at the unconfined state. Images (b) and (d) show the Janus morphology of emulsion droplet upon confinement in aqSDS and aqCTAB. (e) Representative image of a Janus drop and the schematics, depict the balances forces from which the interfacial energy at different interfaces are estimate. (f, g) A complex emulsion was prepared by using Paraffin and Silicone oil as the dispersed

phase and 10 mM aqSDS as the continuous medium. The optical micrographs show that at both confined and unconfined states, the dispersed droplets of oils assume core-shell morphology.

aqueous media	unconfined emulsion		confined emulsion		
	$\gamma_{\text{Sil-aq}}$ (mN/m)	$S = \gamma_{\text{Par-aq}} - \gamma_{\text{Sil-aq}} - \gamma_{\text{Par-Sil}}$ (mN/m)	θ_A (deg)	$\gamma_{\text{Sil-aq}}$ (mN/m)	$S = \gamma_{\text{Par-aq}} - \gamma_{\text{Sil-aq}} - \gamma_{\text{Par-Sil}}$ (mN/m)
1mM SDS	31.0	9.6	133.8 ± 2.6	40.9 ± 0.03	-0.25 ± 0.03
0.3mM CTAB	28.7	9.3	132.3 ± 4.0	38.3 ± 0.04	-0.26 ± 0.04

Table 2: The images as in figure 6(b-d) are used to estimate the interfacial energy, $\gamma_{\text{Sil-aq}}$ at the interface of Silicone and aqueous-surfactant solution at the confined state of the emulsion. The table show also the corresponding $\gamma_{\text{Sil-aq}}$ values at the unconfined state and the spreading coefficient values at both the states.

To examine if similar alteration in morphology was expected for increased concentration of surfactant at the aqueous phase, a complex emulsion was prepared using aqSDS of surfactant concentration 10mM (\gg CMC value of 8.25 mM [23]) as the continuous phase (figure 6f,g); Paraffin and Silicone oil were used as the dispersed phase as before. The liquid pool was confined between two parallel plates as in figure 1. At the unconfined state, with $h > 100 \mu\text{m}$, the dispersed droplets assumed core-shell morphology (figure 6f); and it didn't alter to Janus as the confinement was increased, e.g. h decreased to $\sim 45 \mu\text{m}$, it continued to remain core-shell (figure 6g). Thus, this observation corroborates with earlier observation that presence of micelles dominates over the effect of confinement and as a result, in spite of decrease in pressure within the bulk liquid, driven by its confinement, desorption of surfactant molecules does not happen from the SA interface; and the interfacial energy too doesn't alter.

Summary

While interfacial energy of a solid-liquid or a liquid-liquid interface is generally altered by external means like addition of a surfactant [16, 25], alteration of temperature, pH [26,27] or even UV light induced reforming of a surfactant [17], we have shown here that the same can be accomplished by an alternate method: by tweaking a geometric parameter like confinement of the material (Table 3). In essence, our system consisted of an oil-water interface buried within an aqueous surfactant solution that contains also suspended colloidal particles. We showed that at the unconfined state, the particles were hardly wetted by the interface. However, increase in confinement of the aqueous medium decreased the pressure field within it, which in turn resulted in desorption of surfactant molecules from the oil-water interface. Consequent increase in interfacial energy resulted in enhanced wetting and trapping of the colloidal particles. In similar vein, we demonstrate also alteration in morphology of complex emulsion drops in a multi-phase system: from core-shell to Janus, driven by confinement. While conventional stimuli like temperature, pH or concentration of a dissolved chemical species does change the energy of a buried interface, but in all possibility brings about also undesirable collateral effects like denaturing of a thermally-sensitive molecule [28] or change in inter- or intramolecular interactions and also make those changes irreversible [29], confinement, as shown here, provides a benign mechanism of altering interfacial energy of a specific interface. This mechanism of altering interfacial energy can be relevant for many engineering applications, e.g. micro-nano patterning [30], manufacturing of biomimetic fluidic devices [31], implants for controlled droplet motion, drug delivery, and tunable adsorption [32]; it may also shed light in many biological processes, e.g. transportation and adsorption of molecules on intra-cellular interfaces.

aqueous media	Unconfined State		Confined State	
	$\gamma_{\text{Sil-aq}} _{\text{unconfined}}$ (mJ/m ²)		$\gamma_{\text{Sil-aq}} _{\text{confined}}$ (mJ/m ²)	
	Owens and Wendt Method	SEM images of SiO ₂ particles	Janus emulsion droplets	SEM images of SiO ₂ particles
1mM SDS	31.0	28.6 ± 2.2	40.9 ± 0.03	49.6 ± 9.3
0.3mM CTAB	28.7	33.3 ± 0.5	38.3 ± 0.04	45.4 ± 2.2

Table 3: The interfacial energy values of the silicone – aqueous media interface at the unconfined and confined states are summarized here.

Abbreviations

1. SDS – Sodium Dodecyl Sulfate
2. CTAB - N-Cetyl-N,N,N Trimethyl Ammonium Bromide
3. cSt – Centi Stokes
4. aqSDS – Aqueous solution of SDS
5. aqCTAB – Aqueous solution of CTAB
6. LSR – Liquid Silicone Rubber
7. FC - Trichloro(1H,1H,2H,2H-perfluorooctyl) silane
8. rpm – revolution per minute
9. SEM – Scanning Electron Microscopy
10. DI water – Deionized Water
11. SA interface – Silicone – Aqueous Media Interface
12. $\gamma_{\text{SiO}_2\text{-aq}}$ - interfacial energy of SiO₂ – aqueous medium interface

13. $\gamma_{\text{SiO}_2\text{-Sil}}$ - interfacial energy of SiO_2 – silicone interface
14. $\gamma_{\text{Sil-aq}}$ - interfacial energy of silicone – aqueous medium interface
15. γ_{aqSDS} - surface energy of aqueous SDS solution
16. $\gamma_{\text{Par-aq}}$ - interfacial energy of paraffin – aqueous medium interface
17. $\gamma_{\text{Sil-aq}}$ - interfacial energy of silicone – aqueous medium interface
18. $\gamma_{\text{Par-Sil}}$ - interfacial energy of paraffin – silicone interface
19. S – spreading coefficient
20. CMC – Critical Micelle Concentration

Acknowledgement: AG acknowledges Science and Engineering Research Board (SERB), Government of India for the grant CRG/2021/001287-G and Department of Science and Technology (DST) Government of India for FIST 2013.

References:

1. Maiti, S., Singh, N., & Ghatak, A. (2019, February 18). Confinement-Induced Alteration of Morphologies of Oil–Water Emulsions. *Langmuir*, 35(10), 3797–3804. <https://doi.org/10.1021/acs.langmuir.9b00067>
2. Wang, G., Nguyen, A. V., Mitra, S., Joshi, J. B., Jameson, G. J., & Evans, G. M. (2016, October 1). A review of the mechanisms and models of bubble-particle detachment in froth flotation. *Separation and Purification Technology*. <https://doi.org/10.1016/j.seppur.2016.06.041>

3. Zhao, C. (2013, November 1). Multiphase flow microfluidics for the production of single or multiple emulsions for drug delivery. *Advanced Drug Delivery Reviews*. <https://doi.org/10.1016/j.addr.2013.05.009>
4. Augustin, M. A., & Hémar, Y. (2009, January 1). Nano- and micro-structured assemblies for encapsulation of food ingredients. *Chemical Society Reviews*. <https://doi.org/10.1039/b801739p>
5. Khan, A. Y., Talegaonkar, S., Iqbal, Z., Ahmed, F., & Khar, R. K. (2006, October 1). Multiple Emulsions: An Overview. *Current Drug Delivery*. <https://doi.org/10.2174/156720106778559056>
6. Balaj, R. V., & Zarzar, L. D. (2020, December 1). Reconfigurable complex emulsions: Design, properties, and applications. *Chemical Physics Reviews*. <https://doi.org/10.1063/5.0028606>
7. Raju, R. R., & Koetz, J. (2021, December 24). Pickering Janus Emulsions Stabilized with Gold Nanoparticles. *Langmuir*, 38(1), 147–155. <https://doi.org/10.1021/acs.langmuir.1c02256>
8. Xu, J., Ma, A., Liu, T., Lu, C., Wang, D., & Xu, H. (2013). Janus-like Pickering emulsions and their controllable coalescence. *Chemical Communications*, 49(92), 10871. <https://doi.org/10.1039/c3cc46738d>
9. Kuhar, K., & Ghatak, A. (2022, November 23). Two-Phase Composite Adhesive with Viscoelastic Inclusion. *ACS Applied Polymer Materials*, 4(12), 9095–9102. <https://doi.org/10.1021/acsapm.2c01427>
10. Nagelberg, S., Zarzar, L. D., Nicolas, N., Subramanian, K., Kalow, J. A., Sresht, V., Blankschtein, D., Barbastathis, G., Kreysing, M., Swager, T. M., & Kolle, M. (2017, March 7). Reconfigurable and responsive droplet-based compound micro-lenses. *Nature Communications*, 8(1). <https://doi.org/10.1038/ncomms14673>

11. Mondal, S., Phukan, M., & Ghatak, A. (2015, September 29). Estimation of solid–liquid interfacial tension using curved surface of a soft solid. *Proceedings of the National Academy of Sciences*, 112(41), 12563–12568. <https://doi.org/10.1073/pnas.1502642112>
12. Maestro, A., Guzmán, E., Ortega, F., & Rubio, R. G. (2014, August). Contact angle of micro- and nanoparticles at fluid interfaces. *Current Opinion in Colloid & Interface Science*, 19(4), 355–367. <https://doi.org/10.1016/j.cocis.2014.04.008>
13. Guzmán, E., Ortega, F., & Rubio, R. G. (2022, October 24). Forces Controlling the Assembly of Particles at Fluid Interfaces. *Langmuir*, 38(44), 13313–13321. <https://doi.org/10.1021/acs.langmuir.2c02038>
14. Levine, S., Bowen, B. D., & Partridge, S. J. (1989, January). Stabilization of emulsions by fine particles I. Partitioning of particles between continuous phase and oil/water interface. *Colloids and Surfaces*, 38(2), 325–343. [https://doi.org/10.1016/0166-6622\(89\)80271-9](https://doi.org/10.1016/0166-6622(89)80271-9)
15. Guzowski, J., Korczyk, P. M., Jakiela, S., & Garstecki, P. (2012). The structure and stability of multiple micro-droplets. *Soft Matter*, 8(27), 7269. <https://doi.org/10.1039/c2sm25838b>
16. Zarzar, L. D., Sresht, V., Sletten, E. M., Kalow, J. A., Blankschtein, D., & Swager, T. M. (2015, February 25). Dynamically reconfigurable complex emulsions via tunable interfacial tensions. *Nature*, 518(7540), 520–524. <https://doi.org/10.1038/nature14168>
17. Chevallier, E., Mamane, A., Stone, H. A., Tribet, C., Lequeux, F., & Monteux, C. (2011). Pumping-out photo-surfactants from an air–water interface using light. *Soft Matter*, 7(17), 7866. <https://doi.org/10.1039/c1sm05378g>
18. Beattie, J. K., Djerdjev, A. M., Gray-Weale, A., Kallay, N., Lützenkirchen, J., Preočanin, T., & Selmani, A. (2014, May). pH and the surface tension of water. *Journal of Colloid and Interface Science*, 422, 54–57. <https://doi.org/10.1016/j.jcis.2014.02.003>

19. Vaidya A., Chaudhury M. K. (2002) Synthesis and surface properties of environmentally responsive segmented polyurethanes. *J Colloid Interface Sci* 249(1):235–245.
20. Good, R. J., & Girifalco, L. A. (1960, May). A theory for estimation of surface and interfacial energies. iii. estimation of surface energies of solids from contact angle data. *J. Phys. Chem.*, 64(5), 561–565. <https://doi.org/10.1021/j100834a012>
21. Di, C., Yu, G., Liu, Y., Guo, Y., Sun, X., Zheng, J., Wen, Y., Wang, Y., Wu, W., & Zhu, D. (2009, January 1). Effect of dielectric layers on device stability of pentacene-based field-effect transistors. *Physical Chemistry Chemical Physics*. <https://doi.org/10.1039/b902476j>
22. Jańczuk, B., & Białłopiotrowicz, T. (1989, January). Surface free-energy components of liquids and low energy solids and contact angles. *Journal of Colloid and Interface Science*, 127(1), 189–204. [https://doi.org/10.1016/0021-9797\(89\)90019-2](https://doi.org/10.1016/0021-9797(89)90019-2)
23. Moroi, Y., Motomura, K., & Matuura, R. (1974, January). The critical micelle concentration of sodium dodecyl sulfate-bivalent metal dodecyl sulfate mixtures in aqueous solutions. *Journal of Colloid and Interface Science*, 46(1), 111–117. [https://doi.org/10.1016/0021-9797\(74\)90030-7](https://doi.org/10.1016/0021-9797(74)90030-7)
24. Ruiz, C. C. (1995, October 1). A photophysical study of micellization of cetyltrimethylammonium bromide in urea-water binary mixtures. *Molecular Physics*, 86(3), 535–546. <https://doi.org/10.1080/00268979508629753>
25. Rudin, J., & Wasan, D. T. (1992, August). Mechanisms for lowering of interfacial tension in alkali/acidic oil systems: effect of added surfactant. *Industrial & Engineering Chemistry Research*, 31(8), 1899–1906. <https://doi.org/10.1021/ie00008a010>
26. Li, M., Powell, M. J., Razunguzwa, T. T., & O'Doherty, G. A. (2010, September 17). A General Approach to Anionic Acid-Labile Surfactants with Tunable Properties. *The Journal of Organic Chemistry*, 75(18), 6149–6153. <https://doi.org/10.1021/jo100954q>

27. Yang, Y., Dong, J., Cai, B., Jiang, Z., Cheng, L., & Li, X. (2013). Environmentally responsive adsorption and assembly behaviors from N-alkyl-1,2-ethylenediamines. *Soft Matter*, 9(5), 1458–1467. <https://doi.org/10.1039/c2sm27288a>
28. Mondal, S., Raposo, M. L., Ghosh, A., Prieto, G., Ghosh, S. (2019) Physicochemical and conformational studies on interaction of myoglobin with an amino-acid based anionic surfactant, sodium N-dodecanoyl sarcosinate (SDDS), *Coll. Surf. A* 577, 167–174. <https://doi.org/10.1016/j.colsurfa.2019.05.061>
29. Natarajan, B., Li, Y., Deng, H., L. Brinson, L. C. and Schadler, L. S. (2013), Effect of interfacial energetics on dispersion and glass transition temperature in polymer nanocomposites, *Macromol.* 46 (7), 2833–2841. <https://doi.org/10.1021/ma302281b>
30. Tian, D., Song, Y., & Jiang, L. (2013). Patterning of controllable surface wettability for printing techniques. *Chemical Society Reviews*, 42(12), 5184. <https://doi.org/10.1039/c3cs35501b>
31. Saha, T., Mukherjee, S., Dickey, M. D., & Velez, O. D. (2024). Harvesting and manipulating sweat and interstitial fluid in microfluidic devices. *Lab on a Chip*, 24(5), 1244–1265. <https://doi.org/10.1039/d3lc00874f>
32. Li, N., Xu, Z., Zheng, S., Dai, H., Wang, L., Tian, Y., Dong, Z., & Jiang, L. (2021, May 13). Superamphiphilic TiO₂ Composite Surface for Protein Antifouling. *Advanced Materials*, 33(25). <https://doi.org/10.1002/adma.202003559>

Supporting Information

Confinement induced alteration in interfacial energy

Nitish Singh^{1,#}, Arka Roy^{1,#} and Animangsu Ghatak^{1,2,*}

- [1] Department of Chemical Engineering, Indian Institute of Technology Kanpur, 208016
[2] Center for Environmental Science and Engineering, Indian Institute of Technology Kanpur, 208016 (India)
[*] Prof. A. Ghatak, Corresponding-Author, Author-Three, E-mail: aghatak@iitk.ac.in
[#] Both authors contributed equally

S. no.	Item	Figure	Page no.
1	Section S1: Surface Energy of 0.03 mM aqCTAB	S1	2-3
2	Section S2: Interfacial Energy of silicone – aq. medium for surfactant concentration <u>above CMC</u>	S2	4
3	Section S3(a): Estimation of $\gamma_{\text{Sil-water}}$ before and after confinement		5
4	Section S3(b): Estimation of $\gamma_{\text{Sil-aqSDS}}$ before and after confinement		6
5	Section S3(c): Estimation of $\gamma_{\text{Sil-aqCTAB}}$ before and after confinement		7
6	Section S4: Estimation of $\gamma_{\text{Sil-aqSDS}}$ for different extent of confinement		8
7	References		9

	γ^p (mJ/m ²)	γ^d (mJ/m ²)	$\gamma = \gamma^d + \gamma^p$ (mJ/m ²)	Reference
0.3 mM aqCTAB	39.1	19.6	52.1	measured
1 mM aqSDS	41.9	20.7	62.6	[1]
SiO ₂	28.1	26.0	54.1	[21]
Water	51	21.8	72.8	[22]
Paraffin Oil	0.003	25.5	25.5	[1]
LSR	0.83	23.4	24.2	[1]

Table S1: Surface energy of different chemical species used in experiment. The data show also polar and dispersive component of surface energy.

Phase - 1	Phase - 2	γ_{12} (mJ/m ²)
SiO ₂ particle	water	3.57
SiO ₂ particle	LSR	19.34
SiO ₂ particle	1 mM aqSDS	1.68
SiO ₂ particle	0.3 mM aqCTAB	1.36
LSR	water	38.85
LSR	1 mM aqSDS	31.02
LSR	0.3 mM aqCTAB	28.71
silicone oil	paraffin oil	0.78
paraffin oil	1 mM aqSDS	41.44
paraffin oil	0.3 mM aqCTAB	38.8

Table S2: Interfacial energy between different liquids, estimated by putting polar and dispersive component of surface energy values of respective phases in Owens and Wendt

equation²⁰: $\gamma_{12} = \gamma_1 + \gamma_2 - 2\left(\sqrt{\gamma_1^d \gamma_2^d} + \sqrt{\gamma_1^p \gamma_2^p}\right).$

Section S1. Estimation of surface energy (SE) of 0.03mM aqCTAB solution:

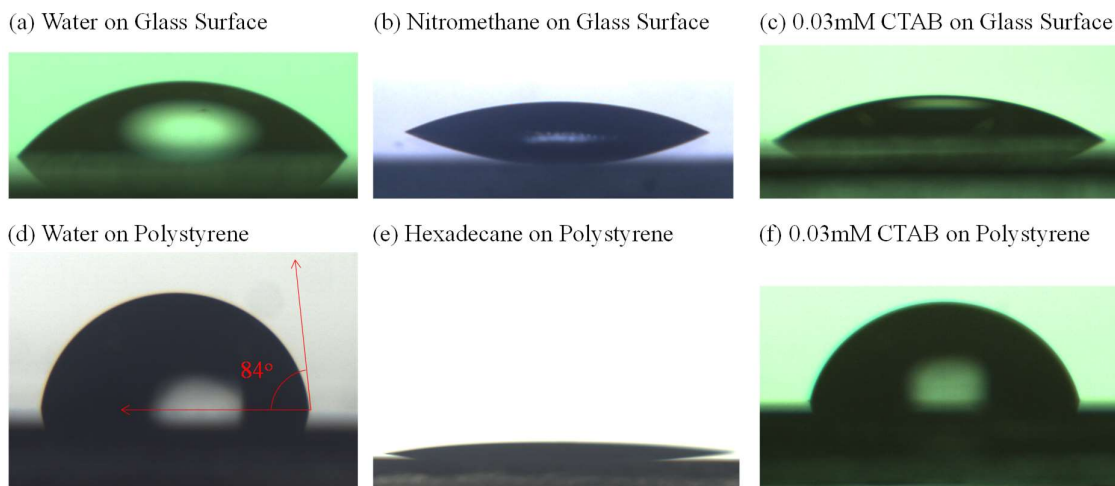


Figure S1: The surface energy (SE) of 0.03mM aqCTAB solution was found out by following the Owens and Wendt method, in which the contact angle of this liquid was to be found out on two solid surfaces of known SE. Polystyrene (PS) and Glass Cover slip (CS) was used for this purpose. However, in order to know their SE, two liquids of known surface energy (both dispersive and polar component) were required to be used. Water and Nitromethane (NM) were used for this purpose. Images (a-c) show sessile drops of water, NM and aqCTAB on CS and (c-e) represent that on the PS respectively.

The contact angles (CA) of water and NM as measured from the above images were first used for estimating the SE of CS and PS respectively. The CAs of 0.03 mM aqCTAB on these surfaces were used for estimating the SE of this liquid. Following equation [1] was used for these calculations, the results from which have been summarized in table S1.

$$(1 + \cos\theta)\gamma_1 = (1 + \cos\theta)(\gamma_1^d + \gamma_1^p) = 2 \left[\sqrt{\gamma_1^d \gamma_2^d} + \sqrt{\gamma_1^p \gamma_2^p} \right]$$

Surface (Phase 2)	Liquid (Phase 1)	γ_1^d (mJ/m ²)	γ_1^p (mJ/m ²)	θ (degree)	γ_2^d (mJ/m ²)	γ_2^p (mJ/m ²)
Polystyrene	Water [2]	21.8	51	84	27.39	4.89
	Hexadecane [3]	27.64	0	8		
Glass Cover Slip	Water [2]	21.8	51	46	0.02	73.14
	Nitromethane [2]	20.3	16.5	23		

Table S1(a): Estimation of dispersive and polar components of SE of PS and CS.

Liquid (Phase 1)	Surface (Phase 2)	γ_2^d (mJ/m ²)	γ_2^p (mJ/m ²)	θ (degree)	γ_1^d (mJ/m ²)	γ_1^p (mJ/m ²)
0.03mM aqCTAB	Polystyrene	27.39	4.89	75	19.6	39.1
	Glass Cover Slip	0.02	73.14	32		

Table S1(b): Estimation of dispersive and polar components of SE of 0.03 mM aqCTAB.

Section S2. Estimation of interfacial energy (IE) of the interface between Silicone and aqueous medium for surfactant concentration exceeding CMC:

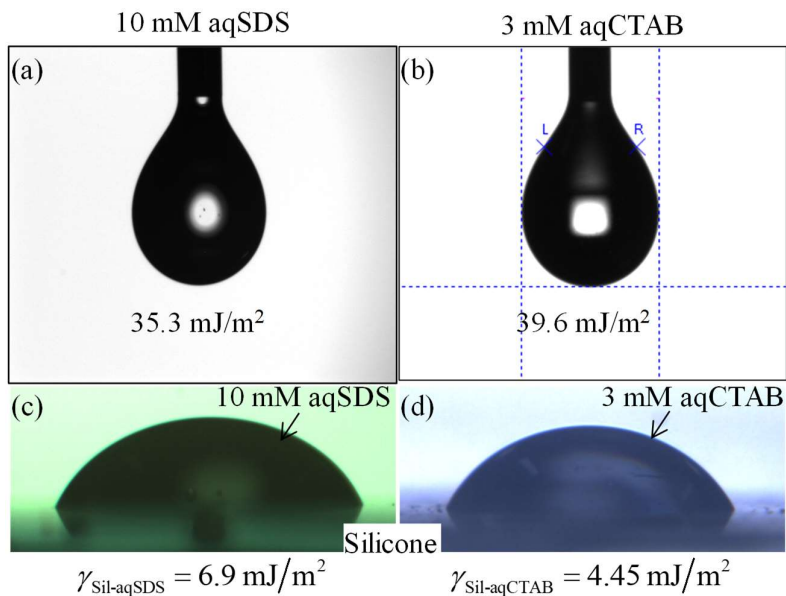


Figure S2: (a, b) Pendant drop method was used to measure the SE of 10mM aqSDS and 0.3mM aqCTAB, which yielded the surface energy of these two liquids as 35.3 mJ/m² and 39.6 mJ/m² respectively. (c, d) Sessile drop of these liquids were dispensed on Silicone surface to measure the advancing equilibrium CA. These CA values were used for estimating the IE of the Silicone-aqueous interface via use of Young's equation.

Section S3a. Estimation of interfacial energy (IE) of silicone and water, $\gamma_{\text{Sil-water}}$ at the unconfined state and at the confined state with $h = 50 \mu\text{m}$:

IE of Silica-Silicone, $\gamma_{\text{SiO}_2\text{-Sil}} = 19.3 \text{ mJ/m}^2$ and Silica-water, $\gamma_{\text{SiO}_2\text{-water}} = 3.6 \text{ mJ/m}^2$ [both from Table 2] and the angle θ as obtained from experiment in figure 4 and 5, were used for estimating $\gamma_{\text{Sil-water}}|_{\text{unconfined}}$ and $\gamma_{\text{Sil-water}}|_{\text{confined}}$ respectively. Table S2(a) presents the data from 4 sets of experiments.

	Unconfined			Confined ($h = 50 \mu\text{m}$)		
S. no.	θ	$\cos(\theta)$	$\gamma_{\text{Sil-water}}$	θ	$\cos(\theta)$	$\gamma_{\text{Sil-water}}$
	degree		mJ/m^2	degree		mJ/m^2
1	63	0.45	34.70	67	0.39	40.30
2	68	0.38	42.03	65	0.42	37.27
3	67	0.39	40.30	66	0.41	38.72
4	69	0.36	43.94	64	0.44	35.93
Average	66.8		40.0	65.5		38.1
Std. Dev	2.6		4.0	1.3		1.9

Table S2a: Summary of calculation leading to estimation of IE of SA interface.

Section S3b. Estimation of IE of silicone and 1 mM aqSDS, $\gamma_{\text{Sil-aqSDS}}$ at the unconfined state and at confined state with $h = 50 \mu\text{m}$:

Interfacial energy (IE) of Silica-Silicone, $\gamma_{\text{SiO}_2\text{-sil}} = 19.3 \text{ mJ/m}^2$ and Silica-aqSDS (1 mM) interface, $\gamma_{\text{SiO}_2\text{-aqSDS}} = 1.7 \text{ mJ/m}^2$ [both data from Table 2] and the angle θ as obtained from experiment in figure 4 and 5 were used for estimating $\gamma_{\text{SiO}_2\text{-aqSDS}}|_{\text{unconfined}}$ and $\gamma_{\text{SiO}_2\text{-aqSDS}}|_{\text{confined}}$.

Table S4(b) presents the data from 3 sets of experiments.

S. no.	Unconfined			Confined ($h = 50 \mu\text{m}$)		
	θ	$\cos(\theta)$	$\gamma_{\text{Sil-aqSDS}}$	θ	$\cos(\theta)$	$\gamma_{\text{Sil-aqSDS}}$
	degree		mJ/m^2	degree		mJ/m^2
1	48	0.67	26.38	66	0.41	43.36
2	52	0.62	28.67	73	0.29	60.28
3	55	0.57	30.77	67	0.39	45.13
Average	51.7		28.61	68.7		49.59
Std. Dev	3.5		2.19	3.8		9.30

Table S2b: Summary of calculation leading to estimation of IE of Silicone-aqSDS (1 mM) interface.

Sample calculation:

$$\gamma_{\text{Sil-aq}} = \frac{\gamma_{\text{SiO}_2\text{-sil}} - \gamma_{\text{SiO}_2\text{-aq}}}{\cos \theta} = \frac{19.3 - 1.7}{\cos(67^\circ)} = 45 \text{ mJ/m}^2$$

Section S3c. Estimation of IE at the interface of silicone and 0.3 mM aqCTAB, $\gamma_{\text{Sil-aqCTAB}}$

at the unconfined state and at the confined state with $h = 50 \mu\text{m}$:

Interfacial energy of Silica-Silicone, $\gamma_{\text{SiO}_2\text{-Sil}} = 19.3 \text{ mJ/m}^2$ and Silica-aqCTAB interface,

$\gamma_{\text{SiO}_2\text{-aqCTAB}} = 1.36 \text{ mJ/m}^2$ [both data from Table 2] and the angle θ as obtained from experiment

in figure 4 and 5 were used for estimating $\gamma_{\text{SiO}_2\text{-aqCTAB}}|_{\text{unconfined}}$ and $\gamma_{\text{SiO}_2\text{-aqCTAB}}|_{\text{confined}}$ respectively.

Table S4(c) presents the data from 3 sets of experiments.

S. no.	Unconfined			Confined ($h = 50 \mu\text{m}$)		
	θ	$\cos(\theta)$	$\gamma_{\text{Sil-aqCTAB}}$	θ	$\cos(\theta)$	$\gamma_{\text{Sil-aqCTAB}}$
	degree		mJ/m^2	degree		mJ/m^2
1	57	0.55	26.38	68	0.38	47.93
2	58	0.53	28.67	66	0.41	44.15
3	57	0.55	30.77	66	0.41	44.15
Average	57.3		33.29	66.7		45.41
Std. Dev	0.6		0.53	1.2		2.18

Table S2c: Summary of calculation leading to estimation of IE of Silicone - aqCTAB (0.3 mM) interface.

Section S4. Estimation of IE at the interface of Silicone and 1 mM aqSDS, $\gamma_{\text{Sil-aqSDS}}$ at different extent of confinement.

IE of Silica-Silicone, $\gamma_{\text{SiO}_2\text{-Sil}} = 19.3 \text{ mJ/m}^2$ and Silica-aqSDS interface, $\gamma_{\text{SiO}_2\text{-aqSDS}} = 1.7 \text{ mJ/m}^2$ [both data from Table 2] and the angle θ as obtained from experiment in figure 5 was used for estimating $\gamma_{\text{Sil-aqSDS}}|_{\text{confinement}}$. Table S4(d) presents the data from 3 sets of experiments.

S. no.	Confinement height, $h = 100 \mu\text{m}$			Confinement height, $h = 70 - 80 \mu\text{m}$		
	θ	$\cos(\theta)$	$\gamma_{\text{Sil-aqSDS}}$	θ	$\cos(\theta)$	$\gamma_{\text{Sil-aqSDS}}$
	degree		mJ/m ²	degree		mJ/m ²
1	58	0.53	33.30	61	0.49	43.36
2	60	0.50	35.29	62	0.47	60.28
3	62	0.47	37.58	64	0.44	45.13
Average	60		35.39	62.3		38.07
Std. Dev	2		2.14	1.5		1.97

Table S3: Summary of calculation leading to estimation of IE of Silicone - aqSDS interface at different extent of confinement.

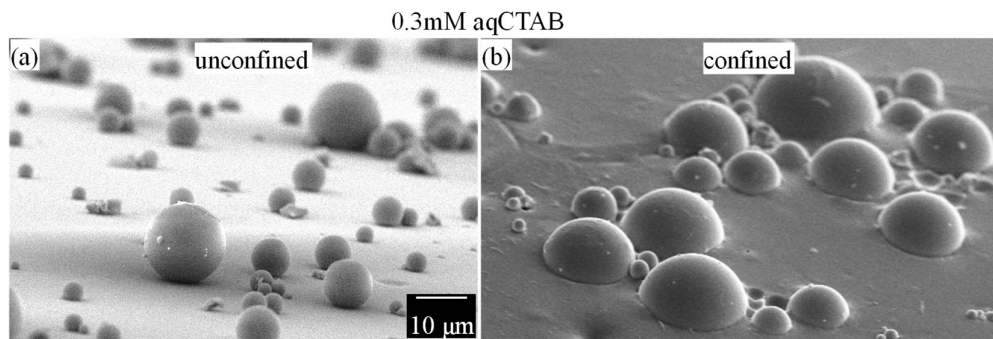


Figure S3: The SEM images show that SiO₂ particles of different sizes get embedded to the silicone lens to similar extent. Here images (a) and (b) represent unconfined and confined state respectively in presence of 0.3 mM solution of aqCTAB.

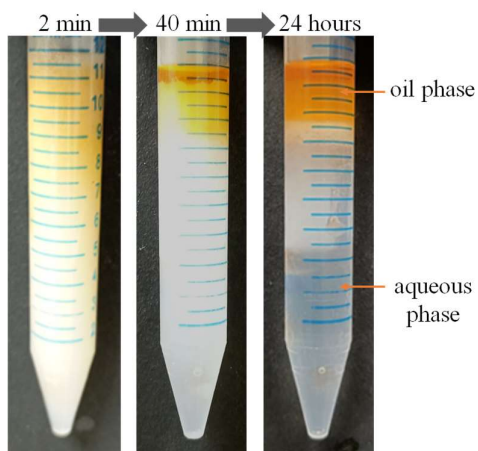


Figure S4. The optical images show that without addition of any surfactant, the emulsion doesn't remain stable leading to phase separation.

Reference:

1. Owens, D. K., & Wendt, R. C., 1969. Estimation of the surface free energy of polymers. *Journal of applied polymer science*, 13(8), 1741-1747.
2. Jańczuk, B., & Białłopiotrowicz, T. (1989, January). Surface free-energy components of liquids and low energy solids and contact angles. *Journal of Colloid and Interface Science*, 127(1), 189–204. [https://doi.org/10.1016/0021-9797\(89\)90019-2](https://doi.org/10.1016/0021-9797(89)90019-2)
3. Rolo, L. I., Caço, A. I., Queimada, A. J., Marrucho, I. M., & Coutinho, J. A. P. (2002, September 28). Surface Tension of Heptane, Decane, Hexadecane, Eicosane, and Some of Their Binary Mixtures. *Journal of Chemical & Engineering Data*, 47(6), 1442–1445. <http://dx.doi.org/10.1021/jc025536+>